Heavy Metals in Polluted White Dwarf G238-44

Nicholas Valles
Andrews University
valles@andrews.edu

Mickey Kutzner
Andrews University
kutzner@andrews.edu
and

Michael Jura
University of California, Los Angeles
jura@astro.ucla.edu

ABSTRACT

We determined the photospheric composition of polluted white dwarf G238-44 from the analysis of far ultraviolet spectra and ascertained physical properties of the star's atmosphere. Previous calculations show that heavy elements should sink out of the star's atmosphere in about three days, however, we discover persistent levels of carbon, nitrogen, oxygen, silicon and iron over nine month time period, which suggests that they are being replenished. The source of this replenishment is yet unknown. Finally, we deduced that, of the elements detected, C II, N II, Si III and Fe III should be the most abundant ions in the photosphere.

As with other polluted white dwarfs, the information garnered from the relative abundances of elements in this dwarf star's atmosphere may soon reveal greater detail about the chemical composition of its extra-solar neighborhood.

Subject headings: DA star, Elements in an Extrasolar System, G238-44, Polluted White Dwarf

1. Introduction

White dwarfs are thought to be the end state for approximately 97% of the stars in our galaxy. They are formed when a main sequence star ends its hydrogen-fusing lifetime, and begins to fuse much heavier elements in its core. If there is insufficient mass to fuse carbon and oxygen to produce heavier elements, these elements can build up in the core of the star. Through the process of stellar evolution, extreme temperatures in the core of the star, radiated the outer layers into space, forming a planetary nebula. After the planetary nebula is shed, the remaining substance is the incredibly hot, dense core of the star, surrounded by a thin insulating photosphere. This astronomical object is known as a white dwarf [Bohm-Vitense, 1989].

Typical white dwarfs have masses on the order of that of the sun, and have radii similar to that of the earth. The tremendous concentration of mass in a small volume means that there are extreme gravitational fields through and around the star. These gravitational fields lead to differentiation which leaves only the lightest elements on the surface of the star. Thus, most white dwarfs have photospheres that only consist of the lightest elements - hydrogen and/or helium, leading to the two main classes of white dwarfs; class DA white dwarfs have hydrogenic photospheres, whereas class DB white dwarfs have only helium present in their atmosphere.

Over the past five to ten years, astronomers have been discovering white dwarf stars that have heavy metals in their photospheres; these are known as polluted white dwarfs. Out of the approximately 9,000 white dwarfs that have been cataloged by the Sloan Digital Sky Survey, there are currently some two-hundred polluted white dwarfs that have been discovered. This paper examines the heavy elements detected in the spectra of a polluted hydrogen (DA) white dwarf star known as G238-44 (EG102, WD1337+705, GW+70° 5824, LTT 18341, PG 1337+705) located at REC 13:38:50.36, DEC 70:17:07.6 (J2000). This study uses data from the FUSE satellite (Far-Ultraviolet Spectroscopic Explorer), which captured spectra in the far ultraviolet band, and seeks to provide a more complete picture as to the elemental abundances in the photosphere of the star.

Finding even small amounts of heavy elements in the usually pure hydrogen atmosphere of this white dwarf is interesting. Since radiative levitation can only keep heavy elements in the photosphere for a few days, persistent elemental abundances suggest ongoing accretion. Using data from the visible and infrared, Holberg showed that the abundance of Mg II in this star is more than can be explained through radiative levitation, which could suggest continuing accretion [Holberg, et. al. 1997]. This study finds the signature of hitherto unidentified elements in the photosphere of the star. By identifying the elements that are contributing to the photospheric pollution and forming a cohesive model with data available from the visible and infrared bands, it may eventually be possible to characterize the source of this pollution and learn more about the surrounding system of this extrasolar neighborhood.

1.1. FUSE Telescope

The Far-Ultraviolet Spectroscopic Explorer was launched June 24, 1999 and was officially decommissioned July 12, 2007. It is designed to acquire spectra in the 905-1187 Å band. There are four apertures that can be used for observation: A large square aperture with a 30 × 30 arcsec field of view, a medium resolution aperture with field of view 4 × 20 arcsec, a high resolution aperture 1.25 × 20 arcsec, and a pinhole aperture 0.5 arcsec in diameter. The large aperture (LWRS) is used for point source observing, and since white dwarfs are very faint objects, G238-44 was observed through the LWRS, which has a resolution of about 100 km s^{-1}, and a resolving power of 20 000.

The satellite has four separate optical channels, consisting of a mirror, Focal Plane Assembly, diffraction grating and a portion of a far ultraviolet (FUV) detector. Two of the four mirrors are coated with SiC which provide reflectivity below 1020 Å. The other two mirrors are coated with a combination of aluminum and Lithium which gives reflectivity above 1050 Å. Each of the FUV detectors are broken into two portions, one covered by SiC and the other by LiF, and each detector approximately cover the entire band. The detector coverage is outlined in Table 2. This gives a total of eight detector/channel combinations that are captured for every observation. While no single detector spans the entire band for most regions, at least two detectors overlap at most bands and the 1015-1075 Å range-where many important weak transitions occur-is covered by all four detectors, providing maximal redundancy.

2. Observations and Data Reduction

The FUSE satellite first observed G238-44 on May 5, 2001 and then made another observation about nine months later on January 27, 2002. Selected data on this star is available in Table 1. The values for mass, $\log g$ and temperature values are from Bergerson, Saffer and Liebert [Bergerson, et. al. 1992]. The value of the radius was derived using the mass-radius relationship for a non-rotating white dwarf, which is used to get an approximation of the density of the star [Schroeder, 1999].

Both exposures were taken through the default aperture, LWRS. The first exposure lasted ≈10.6 ks, while the second exposure was ≈17.4 ks in duration. The data was recorded in time tag mode, which records the coordinates and the nominal time of arrival of each photon within a precision of one second. This provides information necessary for data reduction pipelines to remove noise due to detector walk or data from any bad time periods.

There are eight detector/channel combinations that collectively span the range from 905 - 1180 Å. The data runs, however, were quite noisy at the low end of the band, so the spectrographically useful part of the spectra ranged from approximately 980-1178 Å. Also, the satellite did not observe the target continuously, leading to approximately 30 observations per data run that had to be reduced into a usuable spectrum.

2.1. Spectrum Production

Raw data was processed the CalFUSE v3.0 data reduction pipeline which re-

moved jitters, distortions, performed flat fielding and calibrated the flux and wavelength readings [Dixon, et. al. 2007]. This pipeline resulted in 3-4 calibrated exposures for each of the eight channels.

Calibrated data runs were combined using an IDL routine FUSE_REGISTER, provided by the FUSE collaboration. Leading and trailing zero flux values were masked, so as not to contribute error when combining data. Usual values for flux are on the order of 10^{-12} (ergs/cm^2/s/Å), so points that had values of flux or error $> 10^{-6}$ (ergs/cm^2/s/Å) were removed from the data sample.

To combine the data into a single spectrum, the data was cross-correlated, and when necessary, flux values were scaled to compensate for times when object was not centered in the aperture. Since there is no calibration lamp on board FUSE, the spectra are aligned using the CalFUSE pipeline. Since the pipeline is not perfect, there is still a need to cross-correlate the results.

Cross-correlation is the act of aligning various data runs so that line centers occur at the same position. Adjusting the spectra gives a better signal to noise ratio. An example of uncorrelated data runs is given in Fig. 1. One of the data runs is determined to be the actual center for the absorption line, and the other data runs are shifted to this position, which requires shifts of less than 0.5 Å. Figure 2 demonstrates the effect of combining spectra with and without cross-correlating the data runs. The exposures were then combined using error weighting into a single spectrum to be further analyzed.

2.2. Spectral Measurements

Data from the two data sets were analyzed separately, using LINEPLOT to examine the spectrum Gaussians were fit to each absorption line, and the continuum level was modeled using a constant value, linear or quadratic fit and a gaussian was fit to the absorption line. Finally, the line center, equivalent width, full width at half-maximum and central residual intensity of each line were recorded.

The absorption lines were identified using four resources: Morton's list of resonance lines, the NIST atomic spectra database, Atomic Line List v2.04, and VALD [Morton, 2003; Ralchenko, et. al. 2007; Bautista, et. al. 1999; Kupka, et. al. 2000]. The element identification, lab wavelength and measured wavelength were recorded. Also, when available, the log(gf) and f-value of each transistion was recorded, which is a measurement of the oscillator strength, and is important for photospheric models. Then, the spectral lines present in each of the two data sets were compared.

The spectrum did not appear to be variable, so the spectra from the two data sets were combined with as outlined above, and the process of line measurement and identification was repeated on the final spectrum.

Error in equivalent width is determined by using the formula from Jenkins [Jenkins, et. al. 1973]:

$$\delta EW = \frac{\Delta\lambda M^{1/2}\sigma}{N_c - N_b} \qquad (1)$$

where M is the number of consecutive scans, $\Delta\lambda$ is the wavelength shift of the

line, σ is the standard deviation of the continuum level, N_c is continuum level and N_b is the background count-in in this case taken to be zero.

Finally, we set an upperbound on the amount of argon in the spectrum by trying to fit a the maximum allowable gaussian to the data in the regions where argon is usually detected. This sets an upperbound on the amount of argon in the spectrum, which is important component in determining the contribution of interstellar dust, and thus will serve to help determine if the pollution is due to accretion from a dust cloud moving relative to the star.

2.3. Physical Properties

An important physical property of the star is the electron density that is present in the star's photosphere. This value will be approximated by using the Saha equation, the condition of hydrostatic equilibrium, the equation for the cross section of the hydrogen atom, and the formula for the opacity of the photosphere and solving them simultaneously until a consistent solution is achieved. Written out mathematically we have

$$\frac{n_{i+1}}{n_i} n_e = \frac{2}{\Lambda^3} \frac{g_{i+1}}{g_i} \exp\left[-\frac{E_{i+1}-E_i}{kT}\right] \quad (2)$$

$$P = -\frac{m\nabla\phi}{\chi(n)}\tau \quad (3)$$

$$\sigma(n) = 2.815 \times 10^{29} \frac{G}{n^5\nu^3} \quad (4)$$

$$\chi(n) = \frac{\langle\sigma\rangle}{\langle m_H\rangle}\left[1 - \exp\left(-\frac{h\nu}{kT}\right)\right] \quad (5)$$

Note that $-\nabla\phi$ is the gravitational acceleration, n_e is the electron density, τ is the optical depth, χ is the opacity of the photosphere, G is the Gaunt factor (≈ 2) and Λ is the thermal de Broglie wavelength of an electron (≈ 5.27 Å). The unknown quantities were estimated and then were adjusted until the above equations showed self-consistency. For ν the maximum emitted frequency of light from a blackbody at 20 000 K was used, according to Wein's displacement law. The initial estimates were that for an optical depth of 2/3, the opacity would be approximately 10. A script was written in IDL to cycle through the equations, adjusting in slight increments until the equations were consistent.

3. Analysis

The spectrum corresponding to each observation was analyzed independently. There were 42 absorption lines in each run. Each of the absorption lines had very similar measurements, as demonstrated in Figs. 3, 4 and 5. To further reduce the signal-to-noise ratio, both of the observations were combined into a single spectrum and the absorption lines were measured again. A plot of the final results is shown in Fig. 6.

The absorption lines corresponded to C II, C III, N II, O I, Si II, Si III, Si IV, Fe II and Fe III. It was difficult to accurately measure the oxygen lines because an important oxygen transition line occurs near the emission line of hydrogen from the $n = 3$ state to the $n = 1$ state. Thus, there is less confidence that the photosphere contains oxygen than the other identified ions. The presence of these ions, except for O I, Si II and Si IV, was confirmed by multiple absorption lines. The data for detected absorption lines can be found in Table 3. Also there was an upperbound for the equivalent widths of argon lines of 6.7 mÅ.

Carrying through the IDL script approximating the number density of photospheric electrons, a value of $6.2\times10^{16}e^{-}/cm^{3}$ was obtained. Using this value in the Saha equation, it predicts that, for an effective temperature of 20 000 K, the most abundant species of each element detected should be C II, N II, Si III and Fe III.

4. Conclusions

From the 42 identified absorption lines, there are clear absorption lines corresponding to C, N, O, Si and Fe at wavenumbers corresponding to photospheric temperatures. Thus we deduce that the absorption lines in the spectra is due to elements in the photosphere of G238-44, and not due to cold space dust.

The iterative method employing the Saha Equation to predict the most abundant ions in the photosphere agrees with the ions that have the strongest presence in the spectra, measured by the largest equivalent widths. Specifically, it suggests that C II, N II, Si III and Fe III should be the most abundant ions in the photosphere. Thus the value $n_e = 6.2 \times 10^{16}e^{-}/cm^{3}$ is consistent with experiment.

Theoretical calculations suggest that heavy elements should filter out of the photosphere in a time period of about 3-4 days [Chayer, et. al. 1995]. Though this calculation was done with calcium, the results apply for the heavy elements we are detecting. It is interesting then that the absorption lines in the spectra appeared very similar in the two observations nine months apart. This suggests that there is a sort of equilibrium between the rate that pollution sinks out of the photosphere and the rate of replacement. While Holberg suggests that this could be due to accretion from the interstellar medium by positing that the star is traveling at a speed of 20-40 km s^{-1} relative to a dust cloud of density 1-10 m_H [Holberg, et. al. 1997], currently no cloud has been observed. Furthermore, when examining infrared spectra, there is no infrared excess, making the accretion due to a dusty ring, unlikely.

Determining the relative abundances of elements in the photosphere of the star may assist in infering the source of pollution. For example, if there is approximately 10 parts carbon to one part iron, that ratio is characteristic of comets or stars and could suggest that the pollution is due to accretion from a low mass binary or from comets. However, if this ratio is closer to one part carbon to three parts iron, it would be characteristic of asteriods or a terrestrial planet. In either case, this study will shed light on the elemental composition of this extra-solar system.

5. Further Investigation

The data from this study has been sent to D. Koester at the University of Kiel, Germany. He will model the abundances in the star's photosphere using data from this study, incorporated with data from the IR and UV regions. The final analysis will give important information as to the ratios of various elements present in the star, and what they suggest about their sources in the interstellar neighborhood.

Acknowledgements

The author would like to thank Michael Jura of the Physics and Astronomy Department at the University of California,

Los Angeles for his idea to explore G238-44. The author is also very appreciative to Mickey Kutzner of the Physics Department at Andrews University for the work he contributed refining ideas in this paper and for his advisement. Finally, the author is very grateful for the data processing routines that were written by Don Lindler.

REFERENCES

M. A. Bautista, S. N. Nahar, M. J. Seaton, and D. A. Verner. Atomic Line List (version 2.04). October 1999.

P. Bergeron, R. A. Saffer, and J. Liebert. A spectroscopic determination of the mass distribution of DA white dwarfs. *ApJ*, 394:228–247, July 1992.

Erika Bohm-Vitense. *Introduction to Stellar Astrophysics, Vol. 2*. Cambridge, Cambridge, 1989.

P. Chayer, G. Fontaine, and F. Wesemael. Radiative Levitation in Hot White Dwarfs: Equilibrium Theory. *ApJS*, 99:189–+, July 1995.

W. V. Dixon, D. J. Sahnow, P. E. Barrett, T. Civeit, J. Dupuis, A. W. Fullerton, B. Godard, J.-C. Hsu, M. E. Kaiser, J. W. Kruk, S. Lacour, D. J. Lindler, D. Massa, R. D. Robinson, M. L. Romelfanger, and P. Sonnentrucker. CalFUSE Version 3: A Data Reduction Pipeline for the Far Ultraviolet Spectroscopic Explorer. *PASP*, 119:527–555, May 2007.

J. B. Holberg, M. A. Barstow, and E. M. Green. The Discovery of Mg II λ4481 in the White Dwarf EG 102: Evidence for Ongoing Accretion. *ApJ*, 474:127–130, January 1997.

E. B. Jenkins, J. F. Drake, D. C. Morton, J. B. Rogerson, L. Spitzer, and D. G. York. Spectrophotometric Results from the Copernicus Satellite. V. Abundances of Molecules in Interstellar Clouds. *ApJ*, 181:L122+, May 1973.

F. G. Kupka, T. A. Ryabchikova, N. E. Piskunov, H. C. Stempels, and W. W. Weiss. VALD-2 – The New Vienna Atomic Line Database. *Baltic Astronomy*, 9:590–594, 2000.

D. C. Morton. Atomic Data for Resonance Absorption Lines. III. Wavelengths Longward of the Lyman Limit for the Elements Hydrogen to Gallium. *ApJS*, 149:205–238, November 2003.

Yu Ralchenko, F. C. Jou, D. E. Kelleher, A. E. Kramida, A Musgrove, J. Reader, W. L. Wiese, and K. Olsen. NIST Atomic Spectra Database (version 3.1.3). 2007.

D. V. Schroeder. *Introduction to Thermal Physics*. Addison Wesley Longman, 1999.

This 2-column preprint was prepared with the AAS LaTeX macros v5.2.

A. Appendix - Figures and Images

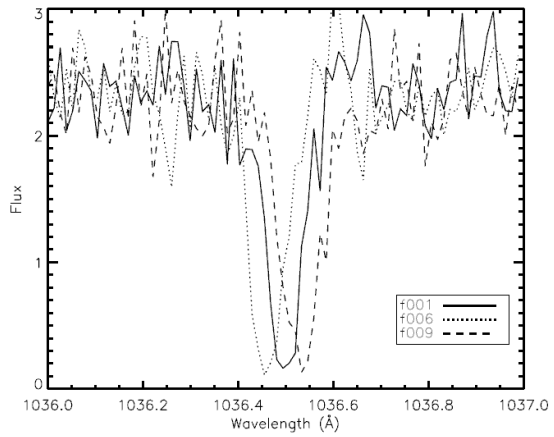

Fig. 1.— Three data runs showing a C II absorption line. The data runs are not correlated, so measurements give misleading values.

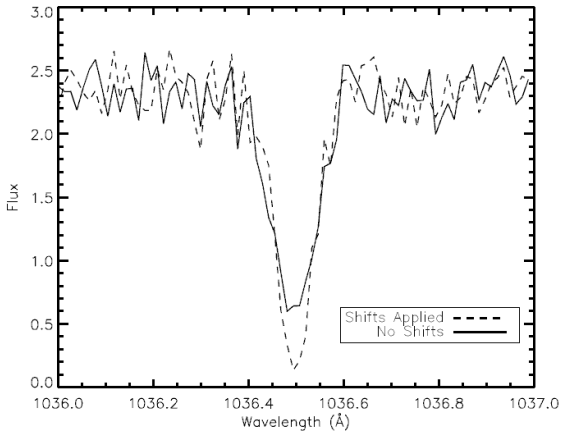

Fig. 2.— The solid line is the result of combining data in figure 1 without performing cross-correlation. The dotted line is the result of cross-correlating line centers to 1036.4 Å, prior to summing data.

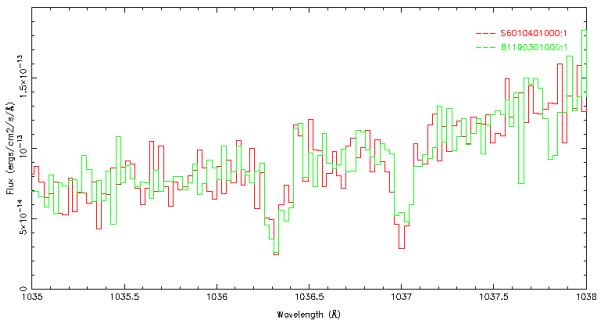

Fig. 3.— Plot showing two absorption lines due to singly ionized carbon from the two data runs taken nine months apart. Observation B119... was taken May 05, 2001, and observation S601... was taken Jan 27, 2002. Note the similar absorption lines in the two data runs.

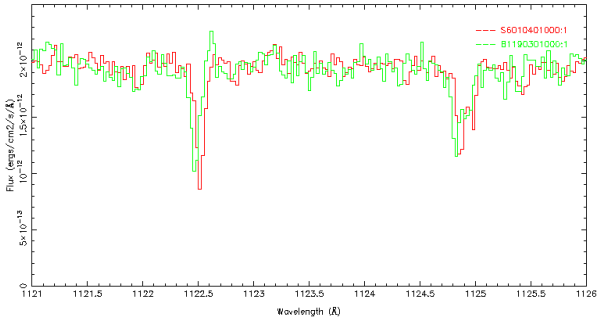

Fig. 4.— Plot showing two absorption lines due to doubly ionized iron from the two data runs taken nine months apart. Observation B119... was taken May 05, 2001, and observation S601... was taken Jan 27, 2002. Note the similar absorption lines in the two data runs.

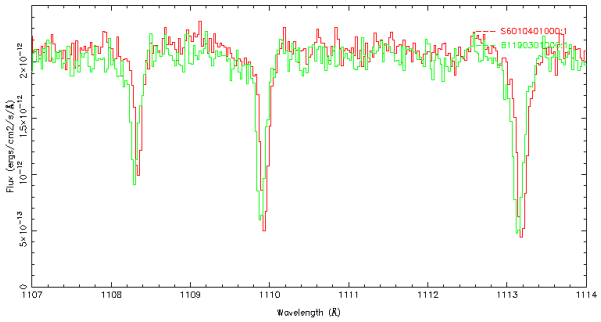

Fig. 5.— Plot showing two absorption lines due to doubly ionized silicon from the two data runs taken nine months apart. Observation B119... was taken May 05, 2001, and observation S601... was taken Jan 27, 2002. Note the similar absorption lines in the two data runs.

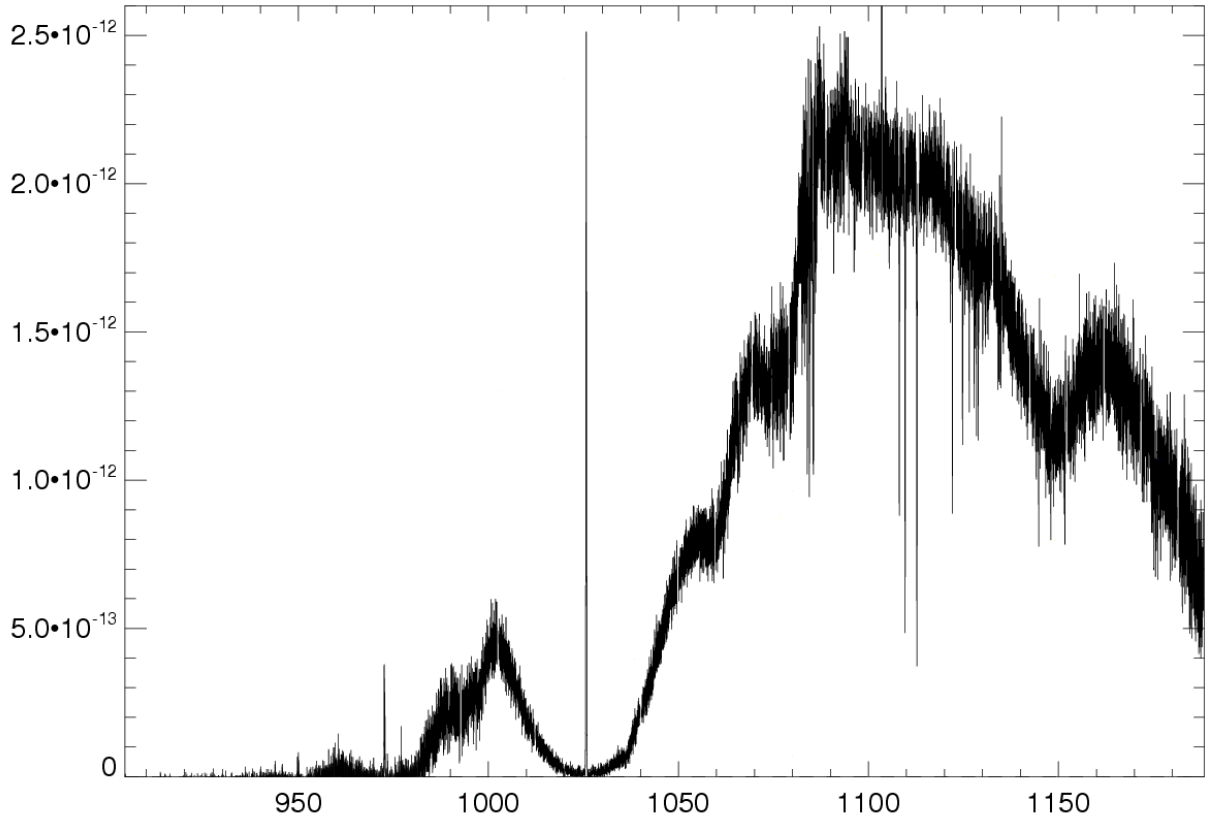

Fig. 6.— A plot of flux (erg/cm^2/s/Å) versus wavelength (Å), made by combining both observations into one. The presence of the large emission line at 1025 Å is due to the $H(n = 3) \rightarrow H(n = 1)$ transition, which is consistent with the fact that G238-44 is a hydrogen white dwarf. The 1080-1130 Å range shows absorption lines due to photospheric silicon and iron.

Table 1

Physical properties of polluted white dwarf G238-44. The values for surface gravity and effective temperature are from Bergeron, Saffer & Liebert (1992). The values for mass, radius and density are computed by using the mass-radius relationship for white dwarfs found in Schroeder (1999) and the surface gravity.

Property	Value
Mass	0.57 $M_\odot$
Radius	1.5 $R_\oplus$
Density	$9.2 \times 10^6 g/cm^3$
Surface Gravity	7.8×10^{10} cm/s^2
T_{eff}	20 230 K

Table 2

Both of the regions from the four detectors are sensitive to FUV light, but each is optimized for light from certain regions. Here we list the sensitivity range of each of the eight channel/detector combinations.

Detector	LiF band (Å)	SiC band (Å)
1A	988 - 1082	1004 - 1090
1B	1095 - 1187	905 - 992
2A	979 - 1074	1017 - 1104
2B	1087 - 1179	917 - 1005

TABLE 3

THIS TABLE LISTS MEASURED ABSORPTION LINE DATA, ALONG WITH PROPOSED ION IDENTIFICATIONS. WAVELENGTHS OF LINE CENTERS ARE GIVEN IN Å. EQUIVILENT WIDTHS AND ERROR IN EQUIVALENT WIDTH IS GIVEN IN mÅ. FULL-WIDTH AT HALF-MAXIMUM IS FOR GAUSSIAN THAT WAS FIT TO THE ABSORPTION LINE AND IS MEASURED IN Å.

$\lambda_{\rm Rest}$	Ion ID	$\lambda_{\rm Obs.}$	EW	δEW	FWHM	CRI	f_{ij}	log gf	dL/L
992.683	Si II	992.7256	70.817	7.30	.118250	.436	0.157	-0.202	12.87
1009.86	C II	1009.8667	10.377	4.89	.035126	.723	0.175	-0.457	1.99
1010.083	C II	1010.0938	21.706	5.30	.078617	.744	0.174	-0.156	3.21
1010.37	C II	1010.3782	24.633	5.28	.079556	.710	0.174	0.020	2.43
1036.3367	C II	1036.3303	52.849	9.65	.080949	.385	0.123	-0.611	-1.85
1037.0182	C II	1037.0100	55.647	7.86	.080271	.353	0.123	-0.310	-2.37
1063.1764	Fe II	1063.1641	10.975	1.70	.084370	.875	0.05475	—	-3.47
1065.88	C II	1065.8703	31.374	1.92	.144852	.798	0.167	0.001	-2.73
1066.133	C II	1066.1427	22.539	1.90	.110755	.809	0.139	-0.255	2.73
1083.9937	N II	1083.9906	40.485	4.50	.092947	.591	0.115	-0.939	-0.86
1084.5841	N II	1084.5724	98.742	4.41	.045271	.570	0.0861	-0.588	-3.23
1085.5511	N II	1085.5425	19.321	4.27	.067960	.736	0.0167	-1.090	-2.38
1085.7096	N II	1085.6933	116.632	4.25	.050508	.595	0.0957	-0.342	-4.50
1096.6073	Fe II	1096.5961	9.363	1.67	.075853	.883	0.02048	—	-3.06
1096.8769	Fe II	1096.8528	11.271	2.41	.077031	.865	0.02027	—	-6.59
1108.37	Si III	1108.3626	104.134	1.76	.059565	.469	0.849	-0.071	-2.00
1109.97	Si III	1109.9562	124.017	1.60	.097550	.264	0.636	0.281	-3.73
1113.23	Si III	1113.2169	159.039	1.59	.130384	.230	0.712	0.551	-3.53
1121.9748	Fe II	1121.9774	9.795	1.81	.068828	.870	0.02898	—	0.69
1122.524	Fe III	1122.5260	49.993	1.82	.084943	.453	0.0797	-0.144	0.53
1124.874	Fe III	1124.9102	55.955	1.64	.168722	.693	0.053	-0.430	9.65
1125.4477	Fe II	1125.4484	10.600	1.81	.085053	.879	0.01558	1.244	0.19
1126.723	Fe III	1126.7319	21.882	1.76	.063659	.676	0.0278	1.322	2.37
1128.05	Fe III	1128.0553	24.625	1.53	.069135	.668	0.0264	1.781	1.41
1128.3400	Si IV	1128.3518	12.290	1.59	.065872	.819	0.734	0.462	3.14
1128.718	Fe III	1128.7270	28.835	1.54	.076764	.643	0.0463	1.546	2.39
1129.191	Fe III	1129.2037	20.040	1.55	.063615	.706	0.0594	0.940	3.37
1130.402	Fe III	1130.4112	17.324	1.52	.074712	.789	0.0792	-1.100	2.44

TABLE 3—*Continued*

$\lambda_{\rm Rest}$	Ion ID	$\lambda_{\rm Obs.}$	EW	δEW	FWHM	CRI	f_{ij}	log gf	dL/L
1131.189	Fe III	1131.1685	25.089	1.96	.189330	.876	0.0198	-1.227	-5.43
1133.4048	Fe II	1133.4276	5.282	2.73	.061086	.918	0.00625	—	6.03
1133.6654	Fe II	1133.6904	10.297	1.81	.106290	.906	0.004715	—	6.61
1144.9379	Fe II	1144.9448	64.884	2.05	.025670	.632	0.08303	—	1.81
1148.0788	Fe II	1148.0795	4.242	2.50	.034756	.889	0.03767	—	0.18
1148.2773	Fe II	1148.2732	61.200	2.51	.015757	.759	0.08279	—	-1.07
1150.6851	Fe II	1150.6939	8.551	2.30	.055441	.854	0.02128	—	2.29
1151.1458	Fe II	1151.1526	10.162	2.29	.049819	.810	0.059	—	1.77
1152.152	O I	1152.1705	35.559	2.09	.101327	.661	0.108	-0.268	4.81
1174.93	C III	1174.9576	21.875	2.64	.101124	.798	0.1136	-0.468	7.04
1175.26	C III	1175.2865	22.748	2.67	.092152	.768	0.2724	-0.565	6.76
1175.71	C III	1175.7150	59.858	2.83	.194596	.715	0.2042	0.009	1.27
1175.99	C III	1176.0171	24.001	2.76	.106052	.788	0.09074	-0.565	6.91
1176.37	C III	1176.3974	15.246	2.80	.067934	.791	0.06807	-0.468	6.98

TABLE 4

UPPERBOUNDS FOR PHOTOSPHERIC ABSORPTION LINES DUE TO ARGON. WAVELENGTHS OF LINE CENTERS ARE GIVEN IN Å. EQUIVILENT WIDTHS AND ERROR IN EQUIVALENT WIDTH IS GIVEN IN mÅ. FULL-WIDTH AT HALF-MAXIMUM IS FOR GAUSSIAN THAT WAS FIT TO THE ABSORPTION LINE AND IS MEASURED IN Å.

$\lambda_{\rm Rest}$	Ion ID	$\lambda_{\rm Obs.}$	EW	δEW	FWHM	CRI	f_{ij}	log gf	dL/L
1048.2199	Ar I	1048.215	6.671	2.54	0.043536246	0.857	0.25	-0.6	-1.41
1066.6599	Ar I	1066.6683	6.610	2.03	0.053046885	0.885	0.067	—	2.36